Optimized Unsymmetrical Per-Phase Droop for Soft Line Switching of Reconfigurable Unbalanced Inverter-Based Islanded Microgrid

Dalia Yousri, Hany E. Z. Farag, *Senior Member, IEEE*, Hatem Zeineldin, *Senior Member, IEEE*, and Ehab El-Saadany, *Fellow, IEEE*

***Abstract*—The legacy of power distribution systems is evolving towards more flexible and dynamically reconfigurable microgrids, which substantially increases line-switching actions. This may introduce undesirable transients, poor reliability, deteriorated power quality, and significant wear and tear in switching devices. Frequent line switching is significant in unbalanced inverter-based islanded microgrids (UIBIM). This article proposes an optimized unsymmetrical per-phase droop-controlled approach to mitigate the influence of line switching during UIBIM reconfiguration and partitioning. To determine the unsymmetrical per-phase Optimal Transitional Droop Settings (OTDS), a new mathematical formulation is modeled to minimize power flow at the switching location(s). Given the unbalanced nature of the system, the proposed unsymmetrical droop will be optimized for each phase independently. The activation start and end instants of the OTDS are selected to reduce the UIBIM dynamics due to the transition between the states due to switching. The superiority and effectiveness of applying the proposed unsymmetrical OTDS are assessed via Matlab/Simulink, utilizing case studies implemented on a 6-bus and an IEEE 34-bus unbalanced systems. The simulation results reveal that the proposed approach can independently minimize the current flow in each phase during the switching process by nearly 98%. Furthermore, the transient voltage during the switching process is significantly reduced.**

***Index Terms*—Per-phase droop control, line-switching, reconfiguration, unbalanced microgrids.**

Manuscript received 29 November 2022; revised 20 March 2023 and 31 July 2023; accepted 28 August 2023. Date of publication 6 September 2023; date of current version 21 February 2024. This work was supported in part by the CIRA-013-2020, Khalifa University, Abu Dhabi, UAE, and in part by ASPIRE through the ASPIRE Virtual Research Institute (VRI) Program, under Award VRI20-07. ASPIRE is part of the Advanced Technology Research Council located in Abu Dhabi, UAE. Paper no. TPWRS-01777-2022. *(Corresponding author: Dalia yousri.)*

Dalia Yousri is with the Advanced Power and Energy Center, EECS Department, Khalifa University, Abu Dhabi 127788, UAE, on leave from the Electrical Engineering, Faculty of Engineering, Fayoum University, Fayoum 63514, Egypt (e-mail: dalia.arashed@ku.ac.ae).

Hany E. Z. Farag is with the Department of Electrical Engineering and Computer Science, York University, Toronto, ON M3J 1P3, Canada (e-mail: hefarag@yorku.ca).

Hatem Zeineldin is with the Advanced Power and Energy Center, EECS Department, Khalifa University, Abu Dhabi 127788, UAE, on leave from the Electric Power Engineering Department, Cairo University, Giza, Egypt (e-mail: hatem.zeineldin@ku.ac.ae).

Ehab El-Saadany is with the Advanced Power and Energy Center, EECS Department, Khalifa University, Abu Dhabi 127788, UAE, and also with the University of Waterloo, Waterloo, ON, Canada (e-mail: ehab.elsadaany@ku.ac.ae).

Color versions of one or more figures in this article are available at https://doi.org/10.1109/TPWRS.2023.3312406.

Digital Object Identifier 10.1109/TPWRS.2023.3312406

NOMENCLATURE

A. Abbreviations

UIBIM	Unbalanced Inverter Based Islanded Microgrids.
OTDS	Optimal transitional droop settings.
DGs	Distributed generators.
PR	proportional-resonant controller.
P	Proportional controller.
L-SHADE	Successful history-based adaptive differential evolution with linear population size reduction.

B. Indices and Sets

i, j	Indices for the network buses.
ij	Indices for the lines.
ϕ	Indices for the phases (a,b,c).
Ω_{ij}^{o}	Set of opened lines.
Ω_{ij}^{cl}	Set of closed lines.
Ω_{ij}^{Droop}	Set of droop-based buses.

C. Notation

$f_i^{P^\phi}(\bullet)$	Active power balance equation for bus i.
$f_i^{Q^\phi}(\bullet)$	Reactive power balance equation for bus i.
$\mid \bullet \mid$	Absolute value of variable $\bullet$.
$\mid \bullet_{\min} \mid$	Minimum limit of variable $\bullet$.
$\mid \bullet_{\max} \mid$	Maximum limit of variable $\bullet$.
$OTDS^*$	Global best OTDS vector.
ⓞ,ⓒⓛ	Opening and closing events.

D. Parameters and variables

K_{pV}, K_{iV}	Proportional and resonant gains of PR voltage control loop.
K_{pI}	Proportional gain of P current control loop.
R_{vir}	Resistive virtual impedance.
ω_c	Cut-off frequency of PR.
V_i^ϕ	Voltage of phase ϕ at bus i.
I_{ij}^ϕ	Per-phase current in line ij.
ω_o	No-load frequency for a DG at bus i.
θ_i^ϕ	Per-phase voltage angle for a DG at bus i.
P_{gi}^ϕ	Generated per-phase active power at bus i.
Q_{gi}^ϕ	Generated per-phase reactive power at bus i.
P_{di}^ϕ	Per-phase active power demand at bus i.
Q_{di}^ϕ	Per-phase reactive power demand at bus i.

© 2023 The Authors. This work is licensed under a Creative Commons Attribution 4.0 License. For more information, see https://creativecommons.org/licenses/by/4.0/

$S^{\phi}_{D^{o}_{ij^{o}}}$	Per-phase magnitude of the apparent power flow in the line ij before opening.
$S^{\phi}_{D^{cl}_{ij^{o}}}$	Per-phase magnitude of the apparent power flow in the line ij during closing.
B^{o}_{ij}, B^{c}_{ij}	Binary inputs for setting the status of the line ij.
$mp^{\phi}_{i}, nq^{\phi}_{i}$	Per-phase droop settings for a DG at bus i, ϕ.
η^{ϕ}_{i}	Selector for droop type of DG i and phase ϕ.
Y_{ij}	Branch ij admittance matrix.
θ_{ij}	Bus admittance angle for branch ij.
t_1, t_3	Instant of activating and deactivating the OTDS, respectively.
t_2	Instant of switching action.
dt_1, dt_2	The time period of activating and deactivating the OTDS, respectively.

I. Introduction

THE high penetration levels of a wide variety of distributed energy resources (DERs) into existing power distribution networks create a path toward having more microgrids, which could be formed at different voltage levels, i.e., medium and low voltages (MV/LV), and switch back and forth between different modes of operation, e.g., grid-connected and islanded [1]. The formation of these microgrids is expected to bring several benefits to the grid operators and customers, such as improvements to system reliability and power quality, a reduction of power losses, and the deferral of grid infrastructure upgrades. Yet, in order to maximize the outcomes of these benefits, the formation of these microgrids needs to be associated with a high degree of system flexibility. The realization of such flexibility could be achieved by different means. Among these, dynamic switching, reconfiguration, and self-healing of these microgrids, i.e., via frequent and automated opening and closing of the system switches over the branches [2], are the most prominent.

Several studies have investigated periodic system reconfiguration in seasonal, weekly, daily, or even hourly schedules for active distribution networks with DERs [3], [4], [5]. However, these studies have not considered the formation of microgrids and their ability to operate in islanded mode. Further, several other research works have proposed the dynamic clustering of power distribution networks into microgrids that are able to switch back and forth between grid-connected and islanded modes of operation [6], [7]. Yet, the main focus of these works is on the determination of the microgrid boundaries to achieve certain system objectives such as loss minimization, self-adequacy, etc., and thus aspects related to system control and line switching during the transition between different states and/or configurations have not been considered.

Most microgrids are dominated by inverter-based DERs. In inverter-based islanded microgrids (IBIM), these DERs control the microgrid (frequency and voltage) and share the load, usually using the droop-controlled scheme [8]. The literature has widely reported that conventional droop control suffers from several deficiencies, including a trade-off between power sharing accuracy and voltage deviation, unbalanced harmonic current sharing, and a high dependency on the line impedance [9]. As such, tremendous research efforts have been carried out over the previous two decades to tackle these challenges via improving and/or optimizing the power-sharing among the DERs. For example, reference [10] constructed the droop equation in a nonlinear form to minimize fuel consumption and reactive power-sharing error. The work in [11] proposed coupling compensation and virtual impedance as a vital component of the control scheme to address the lack of the conventional droop of decoupling ability. The works in [12] identified the droop control settings using a multi-objective optimization approach to enhance the loadability of the IBIM during the reconfiguration process in the steady-state scenarios. Yet the authors did not study the transient issues during the switching action. The authors in [13] stained the light on the importance of updating the droop setting after the reconfiguration process in steady-state scenarios to avoid instability issues occurring after changing the IBIM configuration. It is noticed that the works proposed in this part for identifying the droop setting focus on the steady-state scenarios for enhancing the loadability and minimizing the system's power loss while ignoring the system's transient response during the switching actions. Moreover, the vast majority of previous techniques in the control and optimization of IBIMs were developed and/or tested on balanced power distribution systems. In contrast, in practice, MV/LV power distribution networks are characterized as unbalanced systems, including several single-phase and unbalanced three-phase loads.

In this regard, recent papers have been published to tackle the control challenges of droop-based unbalanced IBIM (UIBIM). For example, power-sharing issues in UIBIMs have been addressed in [14], where an online virtual impedance adjustment strategy was conducted to enhance the imbalance of active and reactive power and unbalanced harmonic power sharing. A modified voltage-current droop control was combined with the model predictive control (MPC) technique to underrate the voltage unbalance and system active power overload [15]. A mixed-integer linear programming (MILP) model was formulated for unbalanced three-phase droop-based IMG for minimizing the generation cost, and the unsupplied demands [16]. The authors in [17] integrated the negative sequence virtual impedance to tackle the conventional droop control drawbacks of inaccurate power sharing among the distributed generators (DGs) due to the feeder/line impedance and the unbalanced loads in UIBIM. Triple-droop control (three inversely symmetrical per-phase droops) was proposed in [18] for managing the real and harmonic power sharing in the LV microgrid under unbalanced and non-linear loads. The work in [19] suggested a symmetrical per-phase power controller for regulating the power-sharing in the grid-connected mode and achieving a smooth transition from grid-tied to islanding operation. It is noted that the above-mentioned control and optimization techniques for both balanced and unbalanced IBIM are specifically developed for normal states of operation (fixed topology) and, thus, their effectiveness hasn't been tested during the transition of IBIM from one state/topology to another via line switching for the purpose of reconfiguring and partitioning the system.

In recent work, the authors in [20] emphasized that careful consideration should be given to the problem of line switching during the transition of low-inertia IBIMs between different states. In particular, frequent line-switching at high current flow in the switched lines (hard switching) causes severe negative effects on IBIMs, including but not limited to: i) poor power quality, shortening of some loads' lifetimes, and harming sensitive electronic loads due to voltage transients (sudden voltage rise or dip) brought on by line-switching processes; ii) triggering the activation of inverter trip signals, which may result in unnecessary system outages, thus, endangering the system's reliability; and iii) wear and tear costs of the line switching devices. Accordingly, one of the promising solutions that could potentially alleviate the prejudicial switching impacts is to minimize the power flow in the lines at which the switching action occurs. With this solution, line switching at low power flows leads to soft switching. Minimizing the power flow in specific lines to achieve soft switching requires changing the power-sharing among the dispatchable DERs. As such, the work in [20] proposed to reduce the current flow over the line at which switching occurs through the deployment of optimal transitional droop settings (OTDS) at the instant of switching. Yet, the application of such an optimization technique is tailored for balanced IBIMs. A simple extension of this technique to unbalanced systems is unlikely, given that UIBIMs might face serious operation challenges when symmetrical three-phase droop control settings are applied. Further, the authors in [20] emphasized only on those cases in which a transient overvoltage occurs due to the imbalance of power-sharing during the line switching, and they paid no attention to the occurrence of a transient undervoltage and the applicability of their proposed control scheme in its mitigation. Indeed, both transient overvoltage and undervoltage could be noticed during the process of line switching and the transition of IBIMs among different states. For this reason, OTDS and control approach must ensure soft switching considering both over- and under-voltage transient occurrences. Most notably, the work in [20] recommends applying the OTDS at the instant of line switching. In this regard, the immediate application of these settings will create a step drop for the power/current flow, which could cause a sudden disturbance, controverting the objective of providing seamless switching.

Aiming to fill in the above-identified research gaps, this paper's contribution is to address the issues associated with the process of line switching in UIBIM-based droop control during reconfiguration and partitioning. To that end, the article proposes the implementation of an optimized per-phase unsymmetrical droop control to force the power-sharing among the DERs in UIBIM systems during the reconfiguration and partitioning processes. Hence, a novel mathematical formulation is introduced to determine the per-phase OTDS needed for the provision of soft line switching while reconfiguring UIBIM. The proposed optimization model is formulated in a generic form, where it is applicable for both balanced and unbalanced IBIM, and it considers any switching action, e.g., opening or closing. In order to achieve a soft transition, the per-phase unsymmetrical OTDS is activated gradually before the instant of line switching. The main contribution of this article is introducing an optimized unsymmetrical per-phase droop-controlled approach in order to minimize the power flow at switching location(s) and, thus, achieve soft line-switching during the reconfiguration and partitioning processes in UIBIMs. To this end, a general mathematical model has been formulated to determine the unsymmetrical per-phase OTDS with consideration of single line-closing, single line-opening, and multiple-line-switching events.

II. Line Switching Transient in UIBIM With Symmetrical Droop Settings

Frequent line switching at high currents may cause undesirable transients and poor power quality for MV/LV microgrids due to their dynamics. The magnitude and impacts of these transients could be exacerbated in systems such as droop-based UIBIM, given their low inertia and high susceptibility to system disturbances. To investigate the transients associated with line switching events for a UIBIM, a 6-bus test system feeding unbalanced three-phase loads, depicted in Fig. 1, is simulated in Matlab/Simulink. The test system has two DGs and a conventional symmetric droop control, with one pair of active and reactive power control settings for each DG, which is considered for controlling the proportional power sharing among the DGs during the switching events. Two switching events are simulated at line L_{56} : event 1 (opening ⓞ) and event 2 (closing ⓒⓛ). The measurement of the three-phase voltages at bus 6 (B6) and the current flow in line L_{56} are recorded and displayed in Figs. 2 and 3 for ⓞ and ⓒⓛ events, respectively. The shown results in Figs. 2 and 3 are displayed per unit with 2 MVA and 4.16 KV base values.

As shown in Fig. 2, a high voltage rise is observed at B6 during event ⓞ because of the switch opening on a high current flow at line L_{56} where DG1 becomes lightly loaded. Such a sudden increase in the voltage magnitude may cause a violation of the IEEE standard 1547.7, which states that the voltage magnitude should not exceed 1.2 pu for a period ranging from 3 to 500 (millisecond) [21]. During event ⓒⓛ of Fig. 3, and without an update in the droop settings, DG1 is required to immediately share the microgrid load with DG2 based on the normal system configuration. In such a case, a deep undervoltage is observed at B6, and a high transient current (more than 10 pu) is withdrawn, where DG1 injects a high current to the system during the transition towards the normal configuration in order to meet its specified power sharing. After more than 0.5 sec, as depicted in Fig. 3(b), the current levels emigrate to the regular operation. Both issues of severe over and under voltage observed during line switching events in UIBIM could cause degradation in the equipment's performance. Consequently, it is essential to implement appropriate control schemes for DGs and optimize their droop settings during line switching events to mitigate undesirable voltage changes and facilitate soft line switching for UIBIM.

III. Proposed Unsymmetrical Per-Phase Droop Control Scheme

Minimizing the flowing of the active and reactive power in switched lines of UIBIM is challenging as the feeding of the line

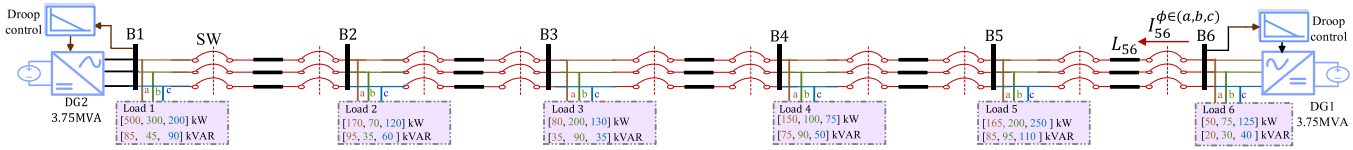

Fig. 1. Unbalanced test system to illustrate the significance of line-switching transients in 6-buses UIBIM.

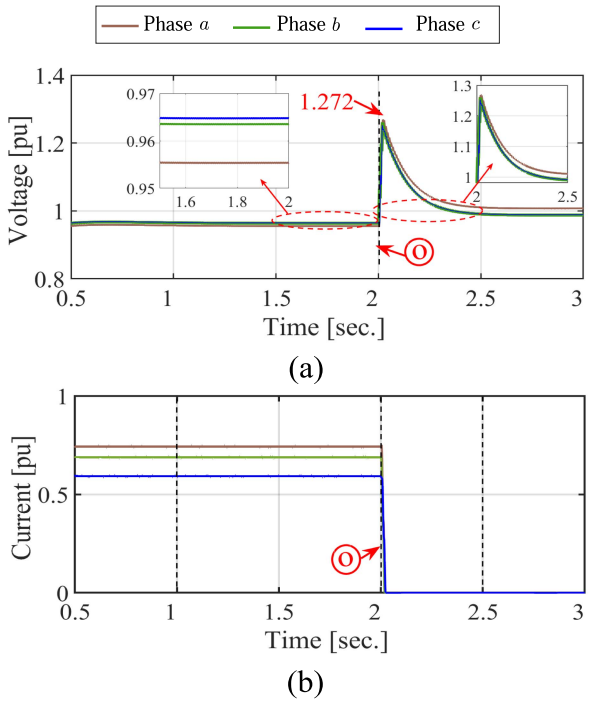

Fig. 2. The dynamic system response before/after the line-opening process ⓞ in UIBIM using conventional symmetric droop control scheme (a) per-phase voltage at bus 6, and (b) per-phase current in L_{56}.

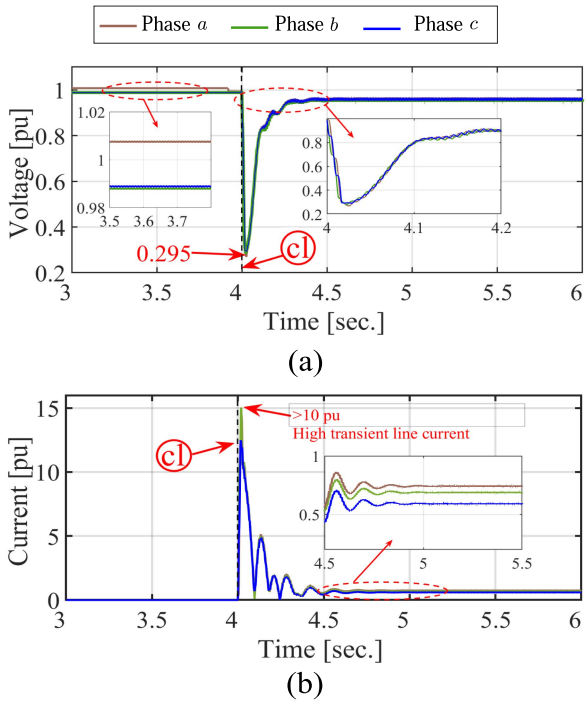

Fig. 3. The dynamic system response before/after the line-closing process ⓒⓛ in UIBIM using conventional symmetric droop control scheme (a) per-phase voltage at bus 6, and (b) per-phase current in L_{56}.

power may be injected from the same or the reverse direction for each phase and with different values, as illustrated in Fig. 4. Accordingly, using the symmetrical conventional droop control is inefficient for handling such a challenge. Therefore, in this work, an unsymmetrical per-phase droop control scheme is implemented to coordinate the injected power of each phase of the droop-controlled DG units in the low-inertia UIBIM separately. The block diagram of the proposed control scheme, shown in Fig. 4, contains a power-sharing control loop, resistive virtual impedance loop, inner voltage, and current control loops. The detailed functions of these loops are described as follows:

In the power control loop, droop control is adopted as it is the most popular power-sharing mechanism among DG units in islanded microgrids. Different droop control formulas are proposed in the literature, which mainly vary based on the system X/R ratio and the output impedance of the DGs [20]. In the case of low voltage (LV) microgrids, which feature highly resistive lines (i.e., X/R $<<$ 1), ($V_i - P_{gi}$ and $d\theta_i - Q_{gi}$) droop control is typically applied, where the voltage/active power droop characteristics are recommended because of the coupling between the V_i and P_{gi} [22]. In contrast, the ($d\theta_i - P_{gi}$ and $V_i - Q_{gi}$), ($d\theta_i - P_{gi} - Q_{gi}$ and $V_i - Q_{gi} - P_{gi}$) formulas are reported as the most adequate droop representation for medium voltage (MV) microgrids [23]. The ($d\theta_i - P_{gi}$ and $V_i - Q_{gi}$) droop characteristics, known as the conventional inductive droop, is widely used assuming a highly inductive microgrid property, i.e., the X/R $>>$ 1 [24]. Meanwhile, when X/R $\approx$ 1, both active and reactive powers are participating in the droop characteristics, i.e., ($d\theta_i - P_{gi} - Q_{gi}$ and $V_i - Q_{gi} - P_{gi}$) that is known as a complex droop [20]. In this work, the unsymmetrical per-phase droop is adopted in a general form represented by ($d\theta_i^{\phi} - P_{gi}^{\phi} - \eta_i^{\phi} Q_{gi}^{\phi}$ and $V_i^{\phi} - Q_{gi}^{\phi} - \eta_i^{\phi} P_{gi}^{\phi}$), ($\phi \in a, b, c, \eta_i^{\phi} \in 0, 1$) to control the active and reactive power of each phase and tackle the coupling issue between the active and reactive powers. To that end, a binary variable (η_i) is defined to offer a flexible selection between the different control approaches. When (η_i) is set to zero, the control scheme follows the ($d\theta_i - P_{gi}$ and $V_i - Q_{gi}$) droop characteristics (X/R $>>$ 1). While η_i is set at one for complex droop (where X/R $\approx$ 1). In the proposed approach, the voltage magnitude and angle of each phase are controlled using

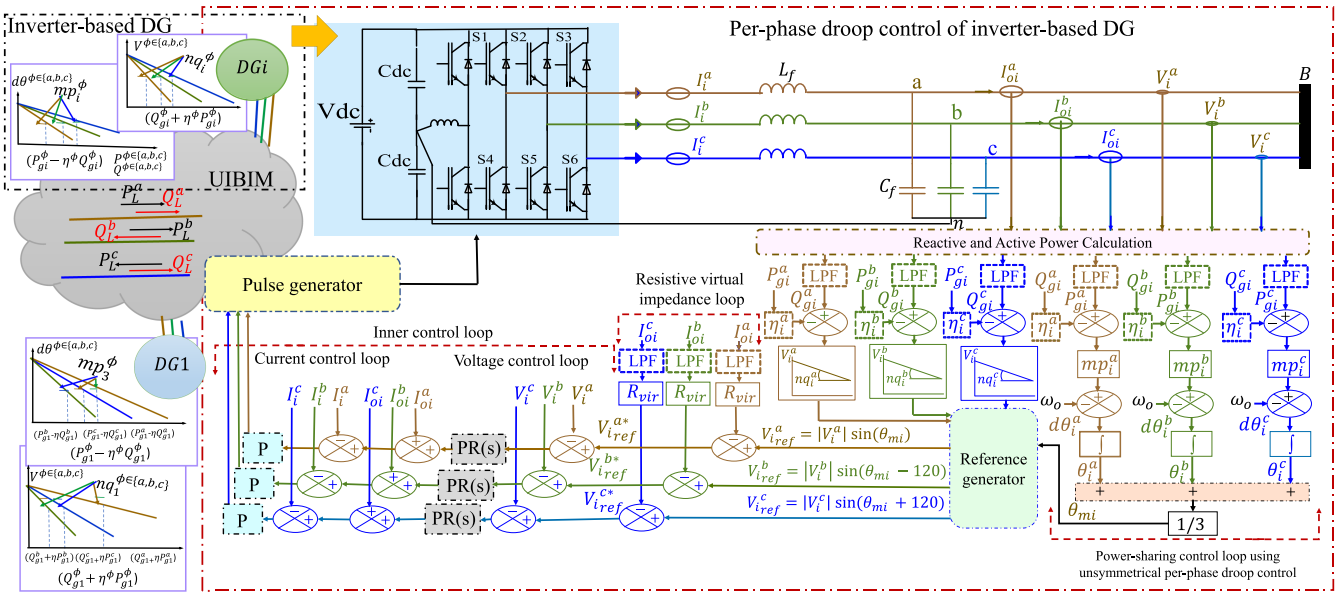

Fig. 4. Schematic diagram of the proposed per-phase droop control of inverter-based DG.

the following mathematical formulations, respectively:

$$V_i^{\phi} = V_o^{\phi} - nq_i^{\phi}\left(Q_{gi}^{\phi} + \eta_i^{\phi} P_{gi}^{\phi}\right) \tag{1}$$

$$d\theta_i^{\phi} = \omega_o - mp_i^{\phi}\left(P_{gi}^{\phi} - \eta_i^{\phi} Q_{gi}^{\phi}\right) \tag{2}$$

where i is a counter that refers to the DG number, ω_o, V_o^{ϕ} are the nominal angular frequency in rad/sec and nominal per-phase voltage, respectively. The η_i^{ϕ} is a binary variable to assign the type of the implemented droop at each ith DG and phase ϕ. This variable is added to model a general control scheme where the $(d\theta_i^{\phi} - P_{gi}^{\phi}$ and $V_i^{\phi} - Q_{gi}^{\phi})$ is implemented for ith DG, and ϕ^{th} phase when the η_i^{ϕ} is 0, whereas the complex droop $(d\theta_i^{\phi} - P_{gi}^{\phi} - Q_{gi}^{\phi}$ and $V_i^{\phi} - Q_{gi}^{\phi} - P_{gi}^{\phi})$ is executed while η_i^{ϕ} is 1. As a result, the type of droop control for each DG and phase can be determined. The per-phase droop coefficients are given by nq_i^{ϕ}, mp_i^{ϕ} for each phase ϕ and ith DG. The voltage angle θ_i^{ϕ} is computed by integrating the droop output $(d\theta_i^{\phi})$ of (2). Then the average value of the per-phase angles is computed for calculating the instantaneous reference voltage values via the following relation:

$$V_{i_{ref}}^{\phi} = |V_i^{\phi}| \sin\left(\theta_{m_i} + \theta_N^{\phi}\right) \tag{3}$$

where θ_N^{ϕ} is the nominal phase angle of specific values $(0, -2/3\pi, 2/3\pi)$. The θ_{m_i} refers to the average value of the per-phase angles of the ith DG $(\theta_{m_i} = \frac{1}{3}\sum_{\phi}\theta_i^{\phi})$.

The proposed per-phase droop control topology is equipped with a resistive virtual impedance loop to regulate the voltage. The fundamental idea is to simulate a voltage drop inside the controller such that the DG perceives the primary network [25]. This target is accomplished by multiplying the resistive virtual impedance (R_{vir}) by each phase's output current (I_o^{ϕ}) and subtracting the result from the computed reference voltage of (3). To filter the oscillatory component of the output current, a low-pass filter (LPF) is added to the resistive virtual impedance, as shown in Fig. 4. Hence, an updated per-phase reference voltage is generated based on the following formula:

$$V_{i_{ref}}^{\phi *} = V_{i_{ref}}^{\phi} - R_{vir} I_o^{\phi} \tag{4}$$

The inner control loop has voltage and current control loops designed to regulate the inverter voltage. In the structured control scheme of Fig. 4, the proportional-resonant controller (PR) is adopted to track the sinusoidal voltage references of each phase of each DG unit, which is brought out of the power control and resistive virtual impedance loops. The transfer function of the PR control can be expressed as follows:

$$PR_i^{\phi}(s) = K_{pV} + \frac{K_{iV}\, s}{s^2 + \omega_c s + \omega_o^2} \tag{5}$$

where K_{pV}, K_{iV} are the proportional and resonant gain factors, respectively. The ω_c, ω_o are the cut-off frequency and resonant frequency, respectively. The output current reference made by the voltage control loop is then applied to the proportional controller in the current control loop to generate the a, b, and c reference voltage for producing the pulse width modulation (PWM) signals of the inverter. The proportional controller transfer function is expressed as follows:

$$P_i^{\phi} = K_{pI} \tag{6}$$

In the proposed control scheme, the a-b-c reference frame is used in the implementation process. The selection of this frame yields remarkable advantages as it can be recognized without any frame conversion, making the system easier to execute and potentially faster.

Implementing the unsymmetrical per-phase droop control scheme to achieve a soft switching requires identifying the OTDS $(nq_i^{\phi}, mp_i^{\phi})$ for each ith DG and ϕ^{th} phase. Therefore, the OTDS identification process is a challenging task as it is needed to determine $2 \times N \times \phi$ variables, where N refers to

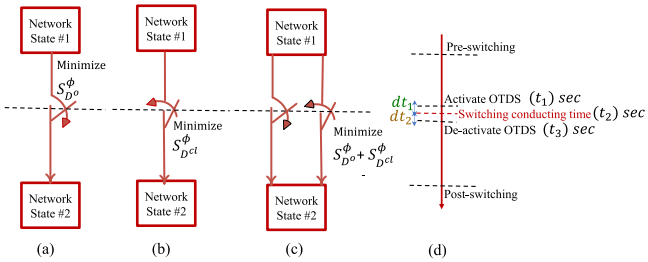

Fig. 5. Schematic diagram for different switching events, (a) Single-line opening (o) event, (b) Single-line closing (cl) event, (c) Multiple-line switching (o, cl), and (d) Action time schedule.

the total number of DGs in the system, ϕ is the total number of phases, factor 2 is used because of calculating two droop parameters, i.e., nq, mp, for each DG. For example, when the system contains 2 droop-controlled DG units, it is required to identify 12 variables for the unsymmetrical-phase droop control settings ($2 \times 2 \times 3$). Accordingly, modeling a reliable and general mathematical formula helps discover the optimization problem landscape and detect the optimal OTDS for different line-switching scenarios.

IV. Formulation of the Proposed Optimization Problem

The aim of this section is to formulate a general mathematical model to determine the OTDS that provide soft line switching via minimization of the power flow in the switched lines of index ij. To that end, two switching types are defined: single-line and multiple-line switching. Fig. 5 shows a schematic diagram for the single-line opening, single-line closing, and multiple-line switching events. As shown in the figure, the proposed model aims to minimize the power flow in the line(s) at which switching occurs. In the single-line opening event depicted in Fig. 5(a), the identified OTDS target the minimization of the pre-switching apparent power flow in each phase ($S^{\phi}_{D^o}$) to avoid the undesirable voltage rise due to a sudden drop in the DG loading. The value of $S^{\phi}_{D^o}$ is computed by solving for the power flow in line ij considering the pre-switching network configuration (state #1). For the closing event presented in Fig. 5(b), the aim is to close the switch with a smooth increase in the line power flow. Hence, the aim of this event is to minimize the power flow of $S^{\phi}_{D^{cl}}$ during the close event of a specific line ij as if the network configuration is in state #2. In the case of multiple-line switching, the system is reconfigured via a number of line-opening and line-closing operations, where pairs of opening and closing operations are simultaneously executed while changing the network topology. Consequently, soft line switching is realized in this case via minimizing the sum of the apparent power flow in these pairs of lines, as illustrated in Fig. 5(c). A planned application of the OTDS has been conducted. As shown in Fig. 5(d), in each line switching event, the UIBIM moves from its current state #1 to a new state #2. The OTDS is activated at instance t_1 while the UIBIM is in state #1 before the occurrence of the line-switching action at t_2. The OTDS is then deactivated at instance t_3 after the UIBIM reaches its new state #2. It is worth mentioning that the activation and deactivation periods, represented by dt_1 and dt_2, respectively, are user-defined parameters. These parameters are defined to avoid a steep drop in the line power flow during the switching event, which, in turn, helps achieve soft line switching. The time periods dt_1 and dt_2, shown in Fig. 5(d), are chosen to provide an adequate time for the UIBIM to readjust the power-sharing among its DGs and reach to steady state before and after the transition of the states due to line switching. Such adequate time is selected to be equal to or more than the settling time, the time required for the response to reach the steady state and stay within the specified tolerance bands around the final value (to settle the power flow in the switched lines to zero or closer to zero before the event instance). The settings of dt_1 and dt_2 are thus determined according to the dynamic response characteristic of the studied microgrid system [26]. Accordingly, a sudden drop or increase in the power flow in the opening and closing events is avoided. The following formula is modeled as a general objective function to obtain the OTDS:

$$\underset{mp_i^{\phi}, nq_i^{\phi}}{\text{Minimize}} \quad S = \sum_{ij^o \in \Omega^o_{ij}} B^o_{ij} \sum_{\phi=a,b,c} S^{\phi}_{D^o_{ij^o}} + \sum_{ij^{cl} \in \Omega^{cl}_{ij}} B^{cl}_{ij} \sum_{\phi=a,b,c} S^{\phi}_{D^{cl}_{ij^{cl}}} \tag{7}$$

where (7) describes a minimization objective function for the apparent power flow in the lines encountering opening and closing events. The variables mp_i^{ϕ}, nq_i^{ϕ} refer to the per-phase droop settings. The symbols of $S^{\phi}_{D^o_{ij^o}}$, $S^{\phi}_{D^{cl}_{ij^{cl}}}$ represent the per-phase apparent power in the line (ij) during the opening state (o) and the closing state (cl), respectively. The input parameters B^o_{ij}, B^{cl}_{ij} have binary values to identify the network switching event as a single line opened ($B^o_{ij} = 1$, $B^{cl}_{ij} = 0$ $\forall_{ij} \in \Omega^o_{ij}$) Fig. 5(a), single line closed ($B^{cl}_{ij} = 1$, $B^o_{ij} = 0$ $\forall_{ij} \in \Omega^{cl}_{ij}$) Fig. 5(b), or the network follows a multiple-line switching event as shown in Fig. 5(c), where ($B^{cl}_{ij} = 1, B^o_{ij} = 1$ $\forall_{ij} \in \Omega^o_{ij}, \Omega^{cl}_{ij}$). The sets $\Omega^o_{ij^o}$, and $\Omega^{cl}_{ij^{cl}}$, in (7), are singletons that refer to lines influenced by the line-opening and closing operations, respectively. The lines that belong to the opening event do not belong to the closing event at the same time; hence there is no intersection between the opening and closing sets ($\Omega^o_{ij} \cap \Omega^{cl}_{ij} = \emptyset$). The optimization problem is subjected to a set of constrained as described below:

- Subject to the power flow equality constraints:

$$f_i^{P^{\phi}}(x_i, x_{gi}) = P^{\phi}_{gi_{\in \Omega^{Droop}}} - P^{\phi}_{di} - \sum_{\substack{j=1 \\ j \neq i}}^{nbr} \sum_{ph=a,b,c} \Big[|V_i^{\phi}||Y_{ij}^{\phi(ph)-n}||V_i^{(ph)}| \cos\left(\theta_{ij}^{\phi(ph)} + \delta_i^{(ph)} - \delta_i^{\phi}\right) - |V_i^{\phi}||Y_{ij}^{\phi(ph)-n}||V_j^{(ph)}| \cos(\theta_{ij}^{\phi(ph)} + \delta_j^{(ph)} - \delta_i^{\phi}) \Big] = 0 \quad \forall_i \forall_{\phi}$$

$$f_i^{Q^{\phi}}(x_i, x_{gi}) = Q^{\phi}_{gi_{\in \Omega^{Droop}}} - Q^{\phi}_{di} - \sum_{\substack{j=1 \\ j \neq i}}^{nbr} \sum_{ph=a,b,c} \tag{8}$$

$$\Big[|V_i^{\phi}||Y_{ij}^{\phi(ph)-n}||V_j^{(ph)}|\sin\left(\theta_{ij}^{\phi(ph)}+\delta_j^{(ph)}-\delta_i^{\phi}\right) -|V_i^{\phi}||Y_{ij}^{\phi(ph)-n}||V_i^{(ph)}|\sin\left(\theta_{ij}^{\phi(ph)}+\delta_i^{(ph)}-\delta_i^{\phi}\right)\Big]=0 \quad \forall_i\forall_\phi \tag{9}$$

$$V_i^{\phi}-V_o^{\phi}+nq_i^{\phi}\left(Q_{gi}^{\phi}+\eta_i^{\phi}P_{gi}^{\phi}\right)=0 \quad \forall_i\in\Omega_i^{Droop} \tag{10}$$

$$d\theta_i^{\phi}-\omega_o+mp_i^{\phi}\left(P_{gi}^{\phi}-\eta_i^{\phi}Q_{gi}^{\phi}\right)=0 \quad \forall_i\in\Omega_i^{Droop} \tag{11}$$

$$V_{i_{ref}}^{\phi*}-V_{i_{ref}}^{\phi}+R_{vir}I_o^{\phi}=0 \quad \forall_i\in\Omega_i^{Droop} \tag{12}$$

$$|\delta_i^a|-|\delta_i^b|-\frac{2\pi}{3}=0 \quad \forall_i\in\Omega_i^{Droop} \tag{13}$$

$$|\delta_i^a|-|\delta_i^c|+\frac{2\pi}{3}=0 \quad \forall_i\in\Omega_i^{Droop} \tag{14}$$

where $f_i^{P^\phi}(x_i,x_{gi})$ and $f_i^{Q^\phi}(x_i,x_{gi})$ are an active and reactive power balance equations for each ith bus and ϕ^{th} phase. The (x_i,x_{gi}) define the state variables at each ith bus. The θ_{ij} in (8)–(9) is the admittance angle for line (ij) and the δ_i denotes the voltage angle at bus i. For each droop-bus i $(i\in\Omega_i^{Droop})$. The (1), (2), (4) are implemented in the power flow constraints as interpreted in (10)–(12) to model the per-phase droop-based buses, and the virtual impedance loop based on the presented works in [27], [28]. For maintaining the phase-shift balance between the three-phase voltage at each droop-based bus, the relations in (13)–(14) are involved in the mismatch equations and are implemented in the control scheme of Fig. 4 by using the reference voltage generator. The power flow equations and constraints have been solved using the Newton trust region presented approach in [27].

- The optimization problem is subjected to additional inequality constraints to set the upper and lower boundaries of the microgrid operation and control parameters, including the system voltage magnitude and angle, system frequency, active and reactive power limits of DGs, and the active and reactive power droop parameters as listed below:

$$V_{i_{\min}}^{\phi}<V_{i,o,c}^{\phi}<V_{i_{\max}}^{\phi} \quad \forall_i\forall_\phi \tag{15}$$

$$\omega_{\min}<\omega_{o,c}<\omega_{\max} \tag{16}$$

$$\delta_{i_{\min}}^{\phi}<\delta_{i,o,c}^{\phi}<\delta_{i_{\max}}^{\phi} \quad \forall_i\forall_\phi \tag{17}$$

$$P_{gi_{\min}}^{\phi}<P_{gi,o,c}^{\phi}<P_{gi_{\max}}^{\phi} \quad \forall_i\forall_\phi \tag{18}$$

$$Q_{gi_{\min}}^{\phi}<Q_{gi,o,c}^{\phi}<Q_{gi_{\max}}^{\phi} \quad \forall_i\forall_\phi \tag{19}$$

$$mp_{i_{\min}}^{\phi}<mp_{i,o,c}^{\phi}<mp_{gi_{\max}}^{\phi} \quad \forall_i\forall_\phi \tag{20}$$

$$nq_{i_{\min}}^{\phi}<nq_{i,o,c}^{\phi}<nq_{gi_{\max}}^{\phi} \quad \forall_i\forall_\phi \tag{21}$$

It is noteworthy that the values of the upper and lower boundaries for the UIBIM operation and control parameters defined in (15)–(21)are set to ensure that the obtained OTDSs will maintain the operation of the UIBIM within the desired operation limits. For example, the boundaries of the voltage magnitudes and system frequency, defined in (15) and (16), respectively, are set based on the applicable standards for voltage and frequency operation limits [29], [30]. Also, the boundaries of the droop parameters defined in (20) and (21) are set to preserve the stability of the microgrid, as illustrated in [31], [32], [33].

For identifying the optimal droop settings that minimize the apparent power flow in the switched lines of (7), successful history-based adaptive differential evolution with linear population size reduction (L-SHADE) algorithm [34] is integrated with the power flow equations. L-SHADE was selected to optimize the OTDS as it proved its reliability and superiority in several real optimization problems. It is ranked the top in one of the most comprehensive competitions of IEEE CEC 2014. Hence, this work applies L-SHADE as a reliable optimizer to minimize the modeled objective function of (7). The following pseudo-code 1 summarizes the main steps while identifying the OTDS based on the L-SHADE algorithm. In the first steps in the pseudo-code 1, the L-SHADE parameters, including; search agents (SA), number of iterations $(T_{\max})$ and control parameters (MF, CMR, CR, F), upper and lower boundaries of the unknown variables (OTDS) are defined. In the initialization process, a set of initial solutions (OTDS) are generated randomly with a dimension of $(SA\times dim)$, where (dim) is the number of the unknown OTDS (for example, dim is 12 for two DGs). For each initial OTDS vector per each search agent $(1\times dim)$, the described UIBIM power flow equations and constraints in (1)–(4), (8)–(21) have been solved using the newton trust region approach in [27] to determine the power flow in the switched line(s). Then the corresponding value of the objective function in (7) has been calculated per each search agent. Throughout the iteration numbers, the initial OTDS sets have been modified based on the L-SHADE structure to fetch the minimal objective function in (7). Since the power flow equations and constraints in (1)–(4), (8)–(21) corresponding to the updated solutions (OTDs) have been recalculated using the newton trust region approach; then the objective function is evaluated. After reaching the maximum iterations $(T_{\max})$, the best solution vector (OTDS*) that corresponds to the minimum objective function is displayed and then applied to the dynamic model of the UIBIM with inverter-based DGs using the control scheme of Fig. 4.

V. Case Studies and Discussions

This section is divided into three subsections to evaluate the performance of the unsymmetrical per-phase control scheme. Subsection A is concerned with providing comparative studies about power-sharing in normal and sudden disturbance conditions. Subsections B and C assess the proposed control scheme and the considered approach for identifying the OTDS in achieving the soft line switching operation. The 6 bus-2DGs system of Fig. 1 is adopted to appraise the performance of the proposed approach for the single-line switching event, while the IEEE 34-bus unbalanced system is embraced for evaluating the proposed approach in cases of multiple-line switching. The time-domain simulations are implemented on Matlab/Simulink, and the optimization problem of identifying the OTDS is solved using a Matlab script. The simulations and analyses are conducted on

Algorithm 1: The Pseudo Code of the L-SHADE for OTDS.

Define: SA is the total number of search agents and $T_{\max}$ is the total number of iterations, UIBIM specifications, Objective function (7).
Define: L-SHADE parameters: archives vector for the mutation factor (MF) and crossover operator (MCR) for storing the average values of the mutation operator (F) and the crossover probability (CR); two sets of SF and SCR to store all CR and F values.
Generate: the initial OTDS, $OTDS = [mp_i^{\phi}, nq_i^{\phi}]$ for each SA.
Compute: Solve the UIBIM power flow equations and the constraints in the ij line using (1), (2), (8)–(21) based on the newton trust region approach in [27] to compute the initial values of the objective function described in (7) by using the initial OTDS.
for $T \leq T_{\max}$ **do**
  for $k \leq SA$ **do**
    Assign random MF_r and MCR_r from the archives vectors of MF and MCR.
    Calculate F^k = Gaussian(MF_r, 0.1).
    Calculate CR^k = Gaussian(CR_r, 0.1).
    Assign the best solution vector $OTDS_T^* = [mp_i^{\phi^*}, nq_i^{\phi^*}]$.
    Select two rand $OTDS^{(r1,r2)}$ vectors from the total SA. $OTDS_T^{(r1,r2)} = [mp_i^{\phi^{r1,r2}}, nq_i^{\phi^{r1,r2}}]$.
    Generate a trial vector based on the following equation [34]: $V_{T+1}^k = OTDS_T^k + F^k(OTDS_T^{r1} - OTDS_T^{r2}) + F^k(OTDS_T^* - OTDS_T^k)$
    Update the solution (OTDS) using crossover operator [34]:
    $u_{T+1}^k = \begin{cases} V_{T+1}^k \; if \; r \; and \leq CR^k \\ OTDS_{T+1}^k \; if \; r \; and > CR^k \end{cases}$
    Solve the UIBIM power flow equations and the constraints in the ij line using (1), (2), (8)–(21) based on newton trust region approach in [27] using the updated solutions.
    Evaluate the objective function of (7) using the updated solutions.
    end for
    Update the SR, SCR, MF. MCR and SA.
end for
Return $OTDS^*$

a personal computer with a Core i7 (2.5 GHz) processor and 16 GB of RAM.

A. Evaluating the Performance of the Proposed Unsymmetrical Per-Phase Droop Control Under Normal and Abnormal Operating Conditions

This subsection investigates the effectiveness of the proposed unsymmetrical per-phase droop control to enhance power-sharing in UIBIM compared to the symmetrical droop control under normal and abnormal operating conditions. The connected DGs in the UIBIM schematic diagram of Fig. 1 supply all the unbalanced three-phase loads until t = 1 sec (normal operating condition). To test the performance of the proposed control under abnormal operating conditions, the loads at phase "c" of all nodes are disconnected until t =1.5 sec [18]. Afterward, loads of phase "c" are restored, and the system returns to its normal operating condition. Fig. 6 shows the active and reactive power-sharing of the DGs for the unsymmetrical per-phase droop control compared to the conventional symmetric droop control under normal and abnormal conditions. To quantify the performance of the implemented control schemes in the steady-state operation, the percentage of active and reactive power error between the desired shared power of DG_i ($(P/Q)_{ref_i}^{\phi}$) and the measured shared power at the ith DG terminal has been calculated using the following formula:

$$\%e_{(p/Q)} = \frac{|(P/Q)_{ref_i}^{\phi} - (P/Q)_{g_i}^{\phi}|}{(P/Q)_{ref_i}^{\phi}} \tag{22}$$

For the time horizon of $t \leq 1$ at normal operating conditions, the ideal active power dispatched from phases "a,b,c" of DG_i are (0.418, 0.354, 0.337) pu, respectively. When the conventional symmetrical droop is applied, Fig. 6(a), the dispatched active power from phases "a,b,c" of DG_1 and DG_2 are (0.388,0.363,0.378) pu and (0.457,0.359,0.311) pu, respectively. Using (22), the percentages of the active power sharing error are (7.177, 2.542, 12.166) % and (9.330, 1.412, 7.715)% for DG_1 and DG_2, respectively. Meanwhile, the measured dispatched active power from phases "a,b,c" of DG_1 and DG_2 are (0.393,0.358, 0.338) pu and (0.419,0.3536,0.333) pu when the unsymmetrical per-phase control scheme is applied as depicted in Fig. 6(c). Accordingly, the percentages of active-power error are (5.981,1.129,0.297) % and (0.239,0.113,1.187)%, respectively. With regard to the reactive power, the percentages of error from phases "a,b,c" of DG_1 and DG_2 extracted from the results of Fig. 6(b) are (15.609,15.012,11.227)% and (16.932,15.012,12.613)% whereas that of Fig. 6(d) are (5.685,12.581,5.664)% and (0.054, 15.199,2.218)% for the symmetrical and unsymmetrical droop, respectively. From these results, it is observed that the implementation of the unsymmetrical per-phase droop control enhances the unbalanced active and reactive power sharing among the DGs in UIBIMs compared to the conventional symmetrical droop control.

For the time of $1 \leq t \leq 1.5$ at abnormal operating conditions, the dispatched active and reactive power from phase "c" of DG_1 and DG_2 are almost equal to zero while using the unsymmetrical per-phase droop control. In contrast, the symmetrical droop control performs improperly to attenuate the circulating active and reactive powers. Moreover, the zoomed curves of the power of phases "a, b" clarify that changing the power of phase "c" has a notable impact on other phases when the symmetrical conventional droop control is applied as illustrated in Fig. 6(a). On the other hand, slight changes in the power of phases "a, b" are observed in Fig. 6(c) when the unsymmetrical per-phase droop control is applied, where it nearly treats each phase separately.

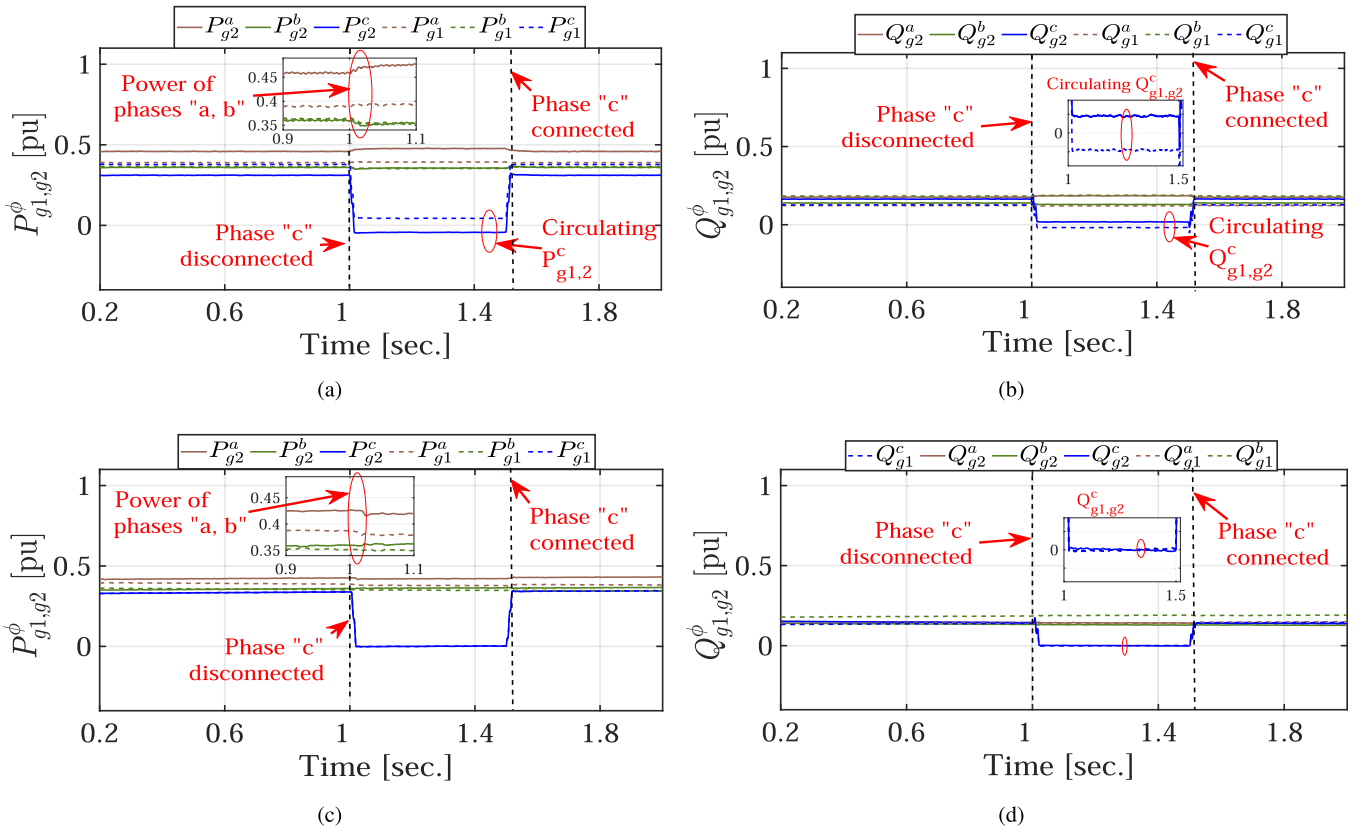

Fig. 6. The DGs active and reactive power-sharing based on (a), (b) conventional symmetrical droop, (c), and (d) unsymmetrical per-phase droop control approaches.

TABLE I
THE IDENTIFIED UNSYMMETRICAL PER-PHASE OTDS IN CASE OF UIBIM WITH 6 BUSES AND 2 DGS

	Phase a	Phase b	Phase c
mp_1^ϕ	8.8924×10^{-6}	9.9276×10^{-6}	5.9213×10^{-6}
nq_1^ϕ	0.2097	0.2692	0.1379
mp_2^ϕ	9.6506×10^{-7}	7.2285×10^{-7}	8.677×10^{-7}
nq_2^ϕ	6.8924×10^{-6}	5.927×10^{-6}	2.0213×10^{-6}

B. Single-Line Switching: UIBIM-6 Buses and 2 DGS Based on Per-Phase Droop Control

In this part, the proposed control scheme is appraised while the line between buses 5 and 6 of Fig. 1 encounters two states of switching: an opening event at a time of 2 sec (viewed as ⓞ) (partitioning process), and a closing event at a time of 4 sec (viewed as ⓒⓛ). The considered droop control scheme is the $(d\theta_i - P_{gi} - Q_{gi}$ and $V_i - Q_{gi} - P_{gi})$ as the X/R ratio nearly equals to 1. The L-SHADE algorithm is adopted to solve the optimization problem formulated in the previous section to determine the OTDS corresponding to minimal flowing power in the switched line for achieving soft switching. The identified OTDS is reported in Table I for the ⓞ and ⓒⓛ events. For exhibiting the dynamic response of the UIBIM while applying the OTDS, the DGS active and reactive power, the injected power to the switched line (L_{56}), and the voltage at bus 6 of the system are traced during the ⓞ and ⓒⓛ events as described below.

Fig. 7 displays the UIBIM's dynamic response for the ⓞ event at $t = 2$ sec. The identified OTDS presented in Table I is applied before the switching action to avoid a sudden drop in the line power flow. For example, it has been observed that applying the OTDS one second before the switching action facilitates seamless readjustment of the power-sharing among the droop-controlled DGs, which in turn, provides smooth decaying of the power flow in the switched line(s). Hence, the OTDS is activated at time 1 sec. as shown in Fig. 7. Fig. 7(a) and (b) illustrate that with activating the OTDS, the generated per-phase active and reactive power from DG1 is reduced gradually; hence, the per-phase active and reactive power flow in line L_{56} is reduced to be less than 98% from the initial one as illustrated from Fig. 7(c). To continuously feed the demand to the MG loads, the per-phase active and reactive power of DG2 is increased as shown in Fig. 7(a), (b) to substitute the lack of the injected power from the DG1 side. In consequence, the power flow in line (L_{56}) is diminished gradually until it reaches nearly zero before opening the line, as depicted in Fig. 7(c), meaning the current flow in the line comes to zero as well. By inspecting the voltage profiles of Fig. 7(d) at time 2 sec, it can be noticed that the improvement in the transient response due to the application of unsymmetrical per-phase OTDS is significant as the switching voltage drops at 0.945 pu compared to 1.272 pu in case of applying conventional symmetrical droop control as illustrated in Fig. 2(a). This is due to the fact that opening the line at near-zero current eliminates the

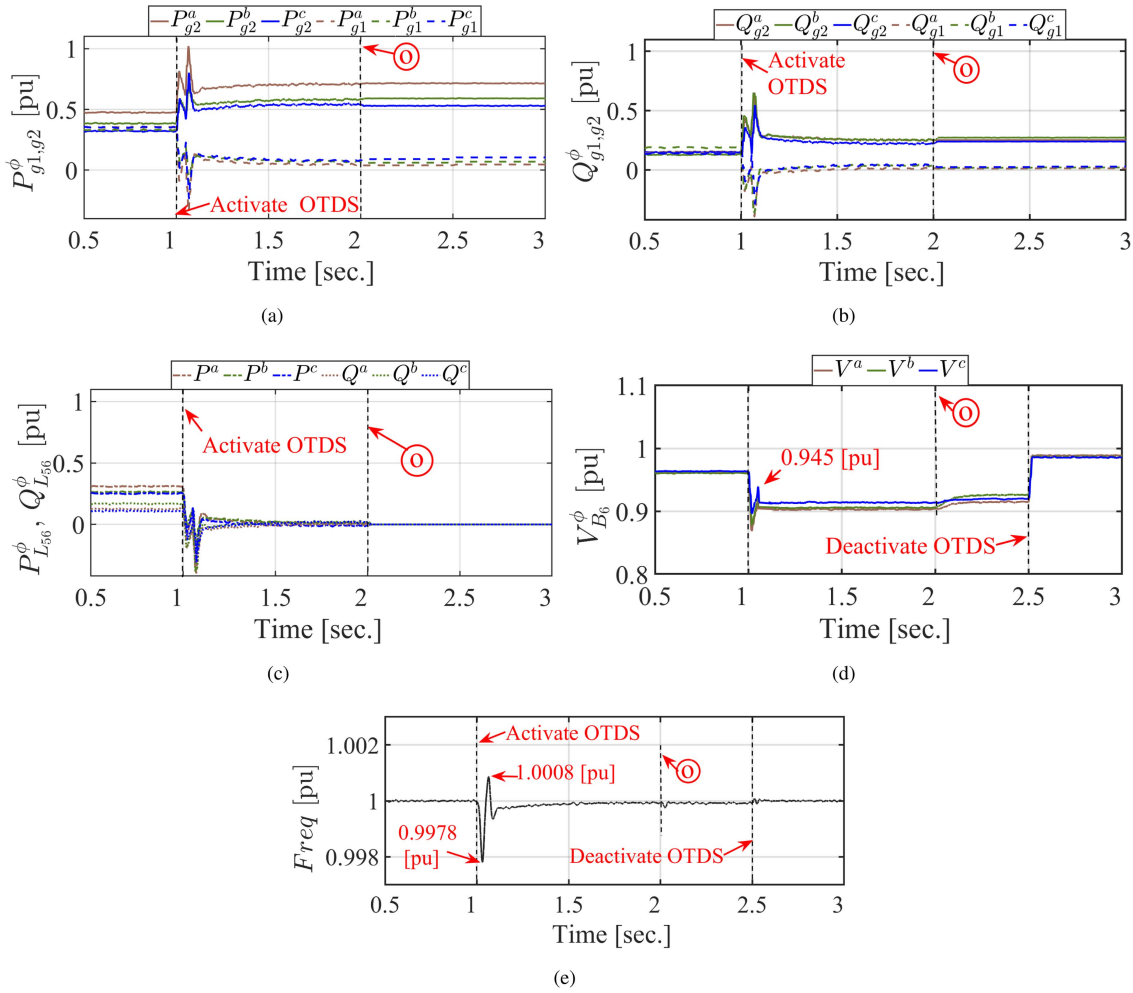

Fig. 7. The UIBIM dynamic response during opening (ⓞ) of the line L_{56} (a) active power of DG1, DG2, (b) reactive power of DG1, DG2, (c) active and reactive power at L_{56}, (d) voltage at bus 6, and (e) ystem frequency while using per-phase droop controlled approach.

voltage rise that was observed previously in the system response of Fig. 2. According to the previous observations, it can be seen that unsymmetrical per-phase OTDS controls the power flow in each phase of the switched line; hence, it helps minimize the unbalanced current flow in each phase separately via re-coordinating the per-phase injected power into the switched lines from the connected DGs in the microgrid. Furthermore, Fig. 7(e) shows that the system frequency varies between 1.0008 pu and 0.9978 pu during the activation time of the OTDS. These changes in the system frequency, which is in the range of +/-0.02%, are within the acceptable steady-state system frequency deviation limits of 3% [30]. The results demonstrate that the process of activating and deactivating the OTDS does not cause issues in the dynamic response of the UIBIM.

For the ⓒⓛ event at $t = 4$ sec. of Fig. 8, the primary target of applying the OTDS of Table I is achieving a nearly zero flowing of power during the closing event to avoid high transient currents flow. Hence the OTDS is applied pre-closing by 500 (milliseconds) before the switching action. The OTDS is deactivated after one second from the closing event (at $t = 5$) after reaching a steady state. Then the operation droop parameters are applied at $t = 5$ sec to return to a UIBIM based 2 DGs configuration. The activation and deactivation periods of the OTDS ensure achieving a smoothing power flow until the getaway from the transient state for reaching smooth steady-state operation. Fig. 8 displays the dynamic response of the UIBIM when line L_{56} encounters the closing event at $t = 4$ sec and OTDS is activated and deactivated at $t = 3.5$, 5 sec, respectively. The DGs' active and reactive power curves of Figs. 8(a),(b) at $3.5 < t < 5$ reveal the effectiveness of the OTDS in keeping on the DGs shared power that achieves zero power flow in the line until reactivating the operational system droop at $t = 5$ sec. In this way, the power flow in the switched line at time 4 sec of Fig. 8(c) is still zero after closing action, which means the OTDS keeps zero current flowing in the line to avoid a high dip in the voltage at bus 6 during the closing event as illustrated in Fig. 8(d). The DGs' active and reactive power after 5 sec of Fig. 8(a) and (b) divulge a smooth power-sharing where the injected per-phase power by the lightly loaded generator (DG1) is increased gradually in front of the DG2 power, which is reduced for re-distributing the shared power among the two DGs. The displayed results illustrate the significant improvements that the unsymmetrical per-phase OTDS provides to the dynamic response of the UIBIM compared with the conventional symmetric droop of Fig. 3. The

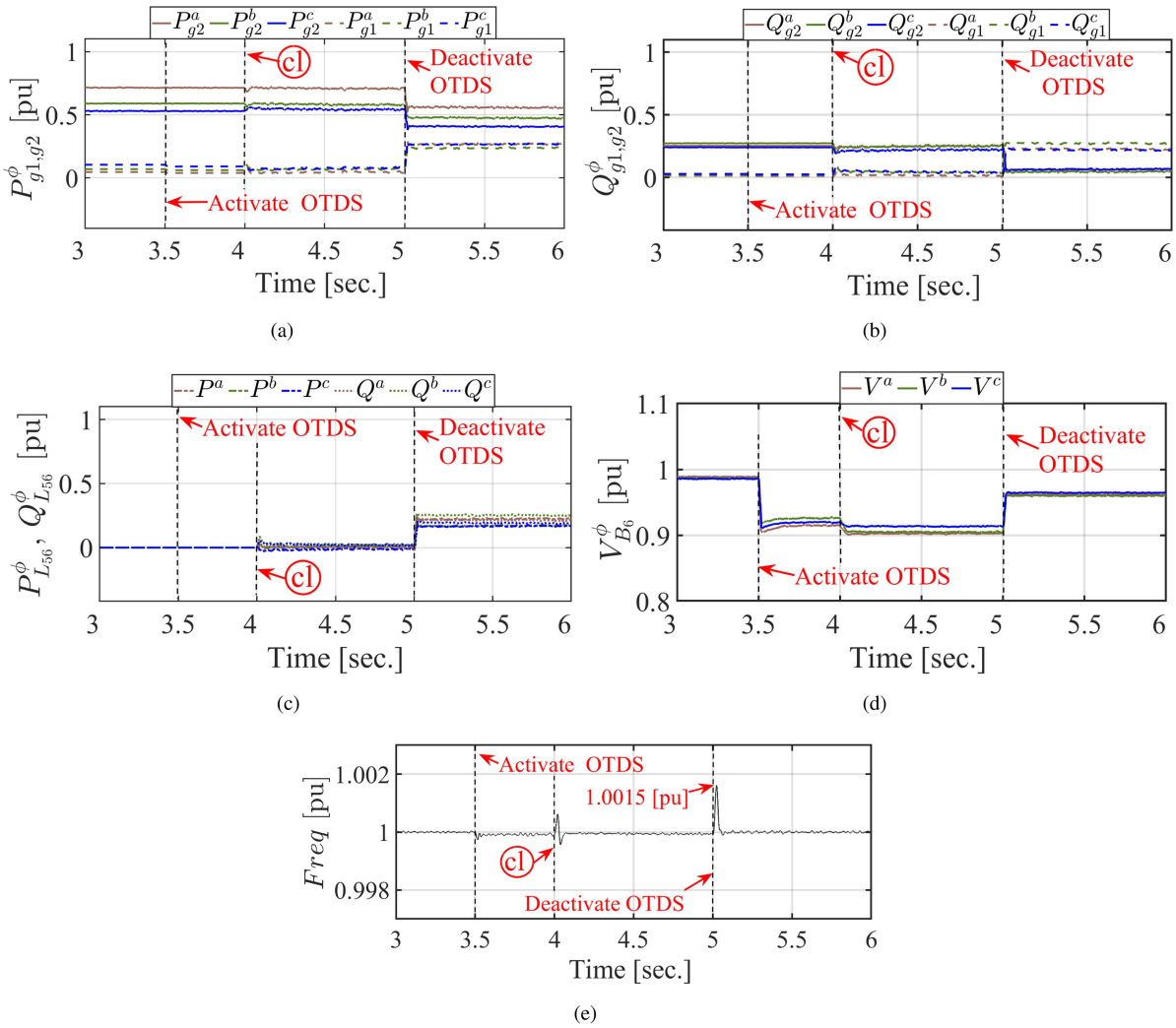

Fig. 8. The UIBIM dynamic response during closing (cl) of line L_{56} (a) active power of DG1, DG2, (b) reactive power of DG1, DG2, (c) active and reactive power at L_{56}, (d) voltage at bus 6, and (d) system frequency while using per-phase droop controlled approach.

power flow in the switched line is smoothly increased; hence the transient current in the case of using the unsymmetrical per-phase droop is kept to be nearly zero after closing; meanwhile, it reaches $>$ 10 pu while using the symmetrical conventional droop as illustrated in Fig. 3(b). Furthermore, unlike the symmetrical conventional sag, which suffers from severe voltage dip during the close switching event, the unsymmetrical per-phase OTDS can maintain the voltage within its prescribed limits during the transition between different network states. As per the system frequency in Fig. 8(e). it is clear that the defined operation constraints in the optimization problem result in seamless activation and deactivation of the OTDS without causing dynamic response issues to the UIBIM. As illustrated in the figure, the maximum measured frequency is found to be 1.0015 pu during the deactivation of the OTDS, which is less than the acceptable standard deviation of 3% [30] from the nominal frequency.

Based on the previous discussions, it is observed that using the unsymmetrical per-phase OTDS mitigates the transients associated with line switching, and thus soft opening and closing events are realized in the UIBIM with 6 buses and 2 DGS without causing issues in the dynamic response of the UIBIM.

C. Sequential Multiple-Line Switching: UIBIM-34 IEEE Bus Based on Per-Phase Droop Control

In this section, the proposed control scheme and the OTDS identification approach performance are examined for sequential actions of multiple-line switching by adopting the IEEE 34-bus unbalanced benchmark system of Fig. 9. The IEEE 34-bus contains different distributed and spotted loads. The load type includes constant current, constant impedance, and constant power models (single- and two-phase loads, and wye/delta-connected three-phase loads) [35]. Three inverter-based unsymmetrical per-phase droop-controlled DGs are connected to the system at buses 808, 832, and 848 through transformers. The depicted configuration of Fig. 9 illustrates the IEEE 34-bus UIBIM with four switches (SW1, SW2, SW3, and SW4). The initial states of the switches are: SW2 and SW4 are closed, while SW1 and SW3 are open. The IEEE 34-bus UIBIM is reconfigured via

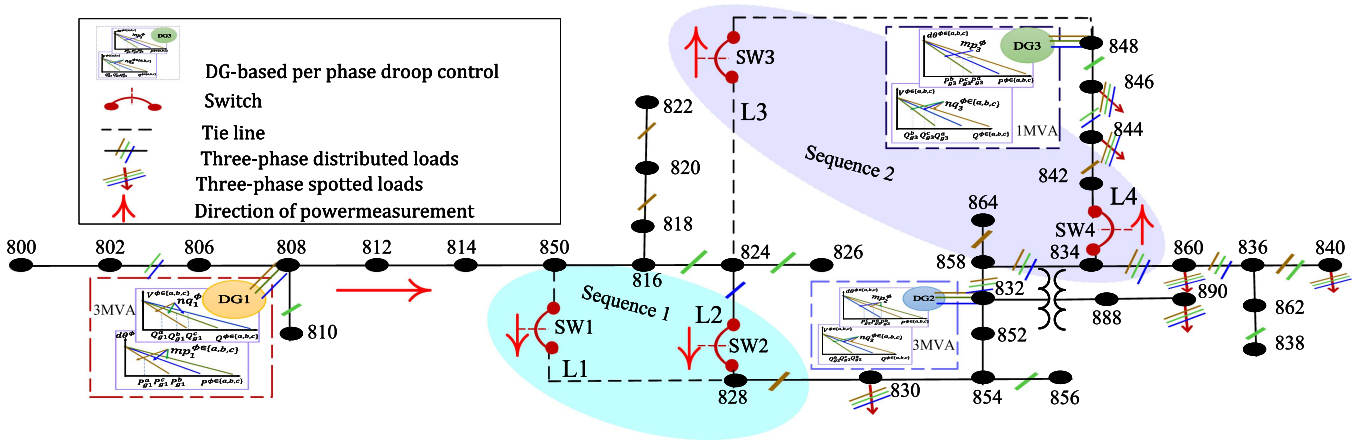

Fig. 9. IEEE 34-bus UIBIM with multiple locations of switches and per-phase droop control of inverter-based DG [36].

TABLE II
THE IDENTIFIED UNSYMMETRICAL PER-PHASE OTDS CONSIDERING SEQUENCE 1 OF THE IEEE 34-BUS UIBIM

	Phase a	Phase b	Phase c
mp_1^{ϕ}	1.0001 $\times 10^{-6}$	8.0619 $\times 10^{-5}$	9.9985 $\times 10^{-5}$
nq_1^{ϕ}	7.0924 $\times 10^{-6}$	6.0094 $\times 10^{-5}$	1.0009 $\times 10^{-4}$
mp_2^{ϕ}	1.0230$\times 10^{-5}$	1.9300 $\times 10^{-5}$	7.8308 $\times 10^{-6}$
nq_2^{ϕ}	9.4618$\times 10^{-5}$	6.2656$\times 10^{-5}$	2.2755$\times 10^{-5}$
mp_3^{ϕ}	6.3265$\times 10^{-5}$	3.7132$\times 10^{-5}$	3.9027 $\times 10^{-5}$
nq_3^{ϕ}	5.0339$\times 10^{-5}$	9.3446$\times 10^{-5}$	5.8007$\times 10^{-5}$

two sequential switching events: in sequence 1, the initial states of (SW1 and SW2) are changed with keeping on the initials state of (SW3 and SW4). Then, in the second sequence, the initial states of (SW3 and SW4) are changed with considering the (SW1 and SW2) states as in sequence 1 to obtain the final construction of the reconfigured IEEE 34-bus UIBIM. The order of the multiple lines switching sequences is based on the works in Ref. [20], as the sequence of the switching that achieves a minimum apparent power flow in the switched lines is the recommended one. By following this strategy, the switching action of (SW1 and SW2) is selected as a first sequence, then the switching action of (SW3 and SW4) in the following sequence. The following subsections present the dynamic response of the IEEE 34-bus UIBIM when implementing sequential multiple-line switching as described above:

1) Sequence 1: Changing Initial States of SW1 and SW2: In this sequence, a pair of two lines are encountered to switch-exchange events simultaneously for providing the first reconfiguration of the IEEE 34-bus UIBIM. For that purpose, the initial states of SW1 and SW2 are changed so that SW1 is closed and SW2 is opened simultaneously at $t = 0.7$ sec. The SW3 and SW4 are kept in their initial state. Towards achieving soft switching, the L-SHADE algorithm is adopted to optimize the proposed objective of (7) to determine the OTDS corresponding to minimal power flow in the pair switched lines $(\sum_{\phi=a,b,c} S^{\phi}_{D^{o}_{(L2)^{o}}} + \sum_{\phi=a,b,c} S^{\phi}_{D^{cl}_{L1^{cl}}})$. The yielded OTDS is listed in Table II. A short period is considered for activating the OTDS before conducting the switching actions to re-distribute the shared power among the DGs and emphasize the soft switching events. Hence, the OTDS is activated at $t = 0.2$ sec. The dynamic response of the test system before and after conducting the first sequence of the reconfiguration process is depicted in Fig. 10. The DGs' generated active and reactive power before and after the switching process are measured and displayed in Fig. 10(a) and (b). Furthermore, the power on the switched lines is measured and plotted in Fig. 10(c) and (d). Based on the indicated direction of the power flow in Fig. 9, the line power is positive when it flows in the same direction as the arrowhead, and it is negative when flowing in the opposite direction to the arrowhead. It is worth mentioning that before applying the OTDS ($t < 0.2$ sec.) of Fig. 10(c), the three DGs were sharing the power flow of $L2$, and hence the measured powers are in positive and negative signs. By inspecting the $L2$ active and reactive power values at ($t < 0.2$ sec), it can be observed that the DG1 injects a significant active power for phases (b,c) to the DG2 and DG3 side. On the other hand, DG1 participates by a bit of the active power of phase (a) for the side of DG2 and DG3. For the reactive power of the three phases (a,b,c), DG2 and DG3 feed the line by remarkable values compared to DG1. Given the complexity of power sharing among the DGs in each phase, minimizing the power flow in this scenario cannot be achieved with symmetrical droop control schemes. Thus, appropriate unsymmetrical phase-independent droop control is paramount. The unsymmetrical per-phase complex droop of (1) and (2) of Section III is the implemented controller in this section.

The recorded active and reactive power of the DGs of Fig. 10(a) and (b) and the power flow in $L2$ of Fig. 10(c) after applying the OTDS before reconfiguration process ($0.2 < t < 0.7$ sec) reveal the effectiveness of using the unsymmetrical per-phase droop control in minimizing the line power by controlling the power of each phase separately. In phase (b), for example, before the switching time, the active power flow in $L2$ comes from the DG1 side; hence it is visualized in positive sign at $t < 0.2$ sec, as shown in Fig. 10(c); hence the proposed control scheme and OTDS works on reducing the injected power of phase (b) from DG1 in front of increasing the production from DG2 and DG3 side as shown in Fig. 10(a) to minimize the power flow of phase (b) through the line. The reactive power flow of phase (b) in the $L2$ is measured in a negative sign, meaning it

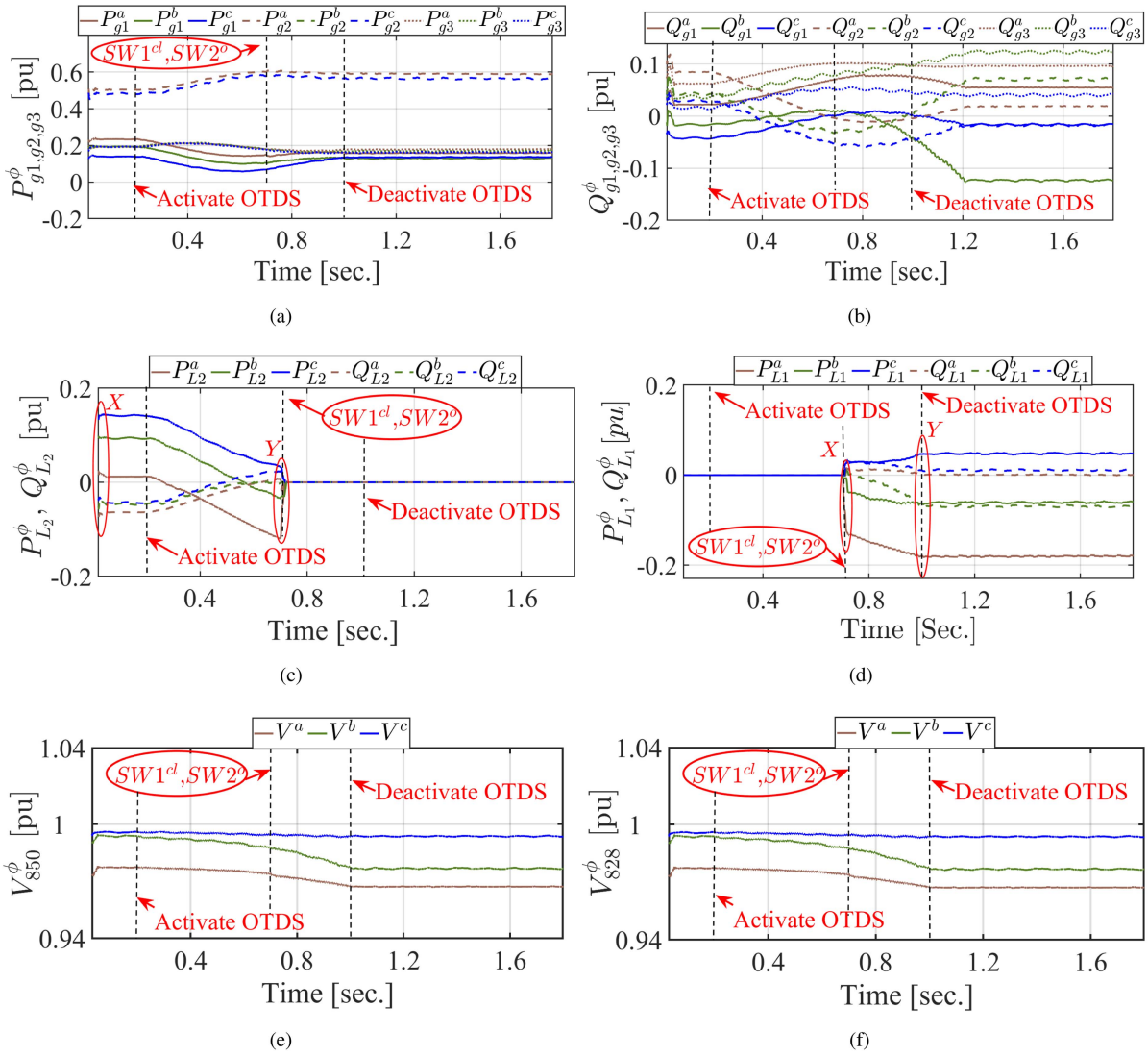

Fig. 10. The IEEE 34 UIBIM dynamic response during the reconfiguration of sequence 1: (a) active power of DG1, DG2, DG3, (b) reactive power of DG1, DG2, DG3, (c) active and reactive power at L_2, (d) active and reactive power at L_1, (e) voltage profile at bus 850, and, (f) voltage profile at bus 828 while using per-phase droop controlled approach.

is supplied from DG2 and DG3 sides (the power flows from the opposite side to the measurement direction). Accordingly, applying the OTDS minimizes the generation from the DG2 and DG3 side instead of increasing the DG1 generation as exhibited in Fig. 10(b) to reduce the transmitted power through the line $L2$. Similarly, for phase (c), the active power flow in the line before switching is injected from DG1 side (it is visualized in positive sign as shown in Fig. 10(a)); hence, the OTDS increases the generation from DG2 and DG3 side to minimize the flow from the DG1. For the reactive power of phase (c), applying unsymmetrical per-phase OTDS shows its superiority in minimizing the injected reactive power from DG2 and DG3 side to reduce the negatively measured reactive power in the line in front of increasing the reactive power contribution from DG1. Following the same concept, the OTDS minimizes the reactive power of phase (a). For the active power of phase (a), the OTDS tries to minimize the active power flow of the phase before the switching action, while phase (a) is highly loaded; hence the DG2 and DG3 contribute a bit for this phase to feed the demand before the reconfiguration process continuously. Applying the OTDS of the unsymmetrical per-phase droop minimizes the apparent power in $L2$ from 0.3 pu at $t < 0.2$ (at point X of Fig. 10(c)) to be 0.165 pu at $t = 0.7$ (at point Y of Fig. 10(c)) before the switching action, accordingly the line power is minimized by nearly 50% before the switching action. Furthermore, applying the OTDS before connecting the tie-line ($L1$) helps in achieving smooth flow for the power through the line until it reaches its steady state value, then the OTDS is deactivated, as illustrated in Fig. 10(d) (at points X, Y, respectively). In the end, this strategy significantly impacts achieving a soft-reconfiguration event at $t = 0.7$ sec and improves the voltage transients produced by the switching operation, as shown in Fig. 10(e) and (f). The displayed three-phase voltages at buses 850 and 828 are being in the standard limits during/after the reconfiguration process. Based on these observations, the unsymmetrical per-phase droop and OTDS prove their ability to control each phase

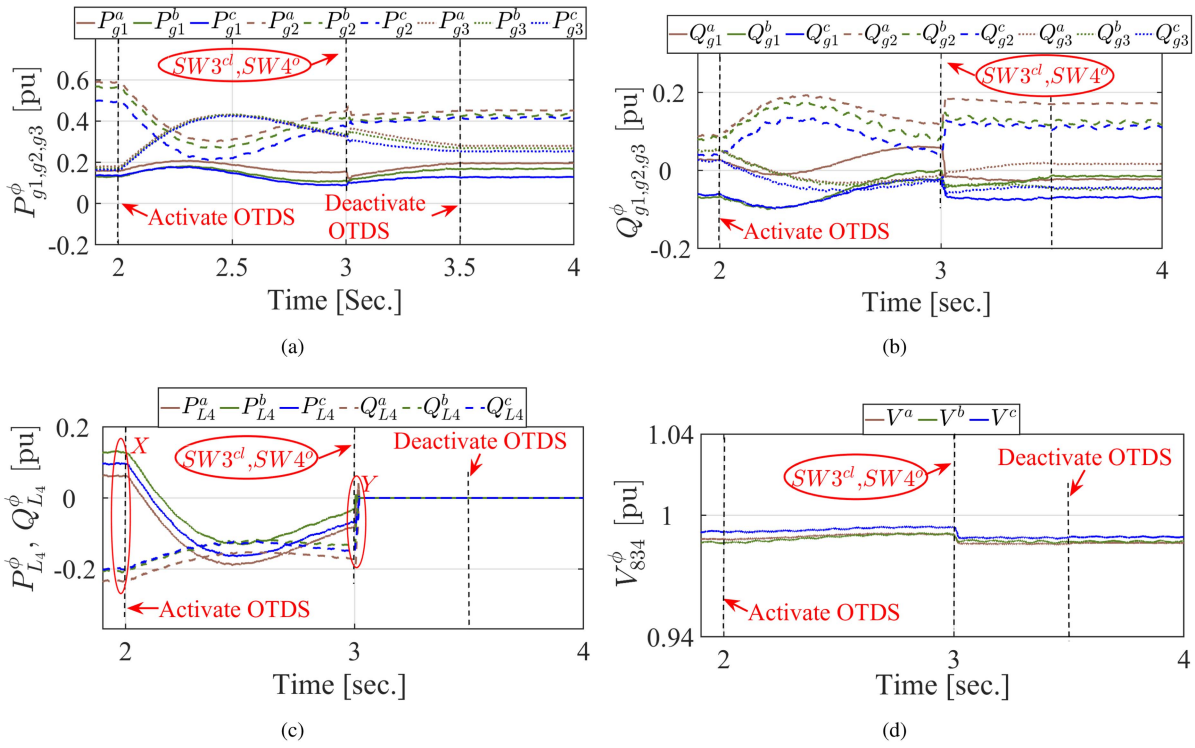

Fig. 11. The IEEE 34 UIBIM dynamic response during the reconfiguration of sequence 2: (a) active power of DG1, DG2, DG3, (b) reactive power of DG1, DG2, DG3, (c) active and reactive power at $L4$, (d) voltage profile at bus 834 while using per-phase droop controlled approach.

TABLE III
THE IDENTIFIED UNSYMMETRICAL PER-PHASE OTDS CONSIDERING SEQUENCE 2 OF THE IEEE 34-BUS UIBIM

	Phase a	Phase b	Phase c
mp_1^{ϕ}	2.4481×10^{-5}	1.9158×10^{-5}	2.6221×10^{-5}
nq_1^{ϕ}	1.7623×10^{-2}	5.2342×10^{-3}	1.0040×10^{-2}
mp_2^{ϕ}	1.0265×10^{-5}	9.4540×10^{-6}	1.9598×10^{-5}
nq_2^{ϕ}	1.2316×10^{-2}	1.1684×10^{-2}	1.0213×10^{-2}
mp_3^{ϕ}	8.1286×10^{-6}	2.0380×10^{-5}	8.1467×10^{-6}
nq_3^{ϕ}	5.7238×10^{-3}	8.8034×10^{-3}	5.1089×10^{-3}

separately to achieve minimum power flow during switching events.

2) Sequence 2: Changing Initial States of SW3 and SW4: This subsection examines the effectiveness of the proposed optimized unsymmetrical per-phase droop with the second sequence of the multiple line switching of IEEE 34-bus UIBIM. In this sequence, the initial state of SW3 and SW4 are exchanged simultaneously, considering the new topology of the IEEE 34-bus UIBIM after implementing sequence 1. Then, the L-SHADE is executed to identify the OTDS that minimizes the power in the switched lines ($L3$, $L4$) using (7) and the updated power flow of the reconfigured IEEE 34-bus UIBIM based on sequence 1. The obtained OTDS is listed in Table III. The dynamic response of the UIBIM before and after implementing sequence (2) of switching is depicted in Fig. 11 to illustrate the DGs active and reactive power, the power in the line $L4$ and the voltage at the 834 bus. The power flow in line $L3$ and voltage at bus 824 are not included in the figure because of the limit in the number of pages. The exhibited Fig. 11(a), (b), and (c) emphasize the superiority of the proposed approach in minimizing the power flow in the switched line of each phase individually hence the apparent power of Fig. 11(c) is minimized from 0.71 pu at point X to 0.48 pu at point Y. Using such approach, the displayed three phase voltages at bus 834 are being in the standard limits during/after the reconfiguration process. Accordingly, a soft reconfiguration process of the IEEE 34-bus UIBIM has been achieved by implementing the unsymmetrical per-phase droop and OTDS.

VI. CONCLUSION

Towards seamless reconfiguration and soft line switching in unbalanced inverter-based islanded microgrids, this article proposes an optimized transitional per-phase unsymmetrical droop control. To that end, a general mathematical formula is modeled for optimizing the transitional per-phase droop settings to minimize the power flow in the switched lines. The formula considers single line-closing, single line-opening, and multiple-line-switching events. The effectiveness of the proposed soft line switching approach is proven for minimizing the power flow in the switched lines considering the 6-bus system and the IEEE 34-bus benchmark system with different switch locations. Regarding a single-line opening event, a significant reduction in the switched power of more than 98 % is attained. This reduction improves the switching operation's voltage transients. Regarding a single-line closing event, a gradual increase in the power flow is achieved that controls the current transients produced by the switching. Finally, considering a multiple-line switching event, using the unsymmetrical per-phase droop control and OTDS proves their ability to minimize the unbalanced power

flow in each phase separately by re-coordinating the per-phase injected power in the switched lines from the connected DGs in the microgrid.

REFERENCES

[1] N. Nasser and M. Fazeli, "Buffered-microgrid structure for future power networks; a seamless microgrid control," *IEEE Trans. Smart Grid*, vol. 12, no. 1, pp. 131–140, Jan. 2021.

[2] W. Zheng, W. Huang, D. J. Hill, and Y. Hou, "An adaptive distributionally robust model for three-phase distribution network reconfiguration," *IEEE Trans. Smart Grid*, vol. 12, no. 2, pp. 1224–1237, Mar. 2021.

[3] F. Ding and K. A. Loparo, "Feeder reconfiguration for unbalanced distribution systems with distributed generation: A hierarchical decentralized approach," *IEEE Trans. Power Syst.*, vol. 31, no. 2, pp. 1633–1642, Mar. 2016.

[4] A. Zhou, H. Zhai, M. Yang, and Y. Lin, "Three-phase unbalanced distribution network dynamic reconfiguration: A distributionally robust approach," *IEEE Trans. Smart Grid*, vol. 13, no. 3, pp. 2063–2074, May 2022.

[5] S. F. Santos, M. Gough, D. Z. Fitiwi, J. Pogeira, M. Shafie-khah, and J. P. Catalão, "Dynamic distribution system reconfiguration considering distributed renewable energy sources and energy storage systems," *IEEE Syst. J.*, vol. 16, no. 3, pp. 3723–3733, Sep. 2022.

[6] G. G. Talapur, H. M. Suryawanshi, L. Xu, and A. B. Shitole, "A reliable microgrid with seamless transition between grid connected and islanded mode for residential community with enhanced power quality," *IEEE Trans. Ind. Appl.*, vol. 54, no. 5, pp. 5246–5255, Sep./Oct. 2018.

[7] M. Awal, H. Yu, H. Tu, S. M. Lukic, and I. Husain, "Hierarchical control for virtual oscillator based grid-connected and islanded microgrids," *IEEE Trans. Power Electron.*, vol. 35, no. 1, pp. 988–1001, Jan. 2020.

[8] J. M. Guerrero, J. C. Vasquez, J. Matas, L. G. D. Vicuña, and M. Castilla, "Hierarchical control of droop-controlled AC and DC microgrids–A general approach toward standardization," *IEEE Trans. Ind. Electron.*, vol. 58, no. 1, pp. 158–172, Jan. 2011.

[9] Y. Han, P. Shen, X. Zhao, and J. M. Guerrero, "An enhanced power sharing scheme for voltage unbalance and harmonics compensation in an islanded AC microgrid," *IEEE Trans. Energy Convers.*, vol. 31, no. 3, pp. 1037–1050, Sep. 2016.

[10] A. Elrayyah, F. Cingoz, and Y. Sozer, "Construction of nonlinear droop relations to optimize islanded microgrid operation," *IEEE Trans. Ind. Appl.*, vol. 51, no. 4, pp. 3404–3413, Jul./Aug. 2015.

[11] Z. Peng et al., "Droop control strategy incorporating coupling compensation and virtual impedance for microgrid application," *IEEE Trans. Energy Convers.*, vol. 34, no. 1, pp. 277–291, Mar. 2019.

[12] M. M. A. Abdelaziz, H. E. Farag, and E. F. El-Saadany, "Optimum reconfiguration of droop-controlled islanded microgrids," *IEEE Trans. Power Syst.*, vol. 31, no. 3, pp. 2144–2153, May 2016.

[13] D. K. Dheer, O. V. Kulkarni, S. Doolla, and A. K. Rathore, "Effect of reconfiguration and meshed networks on the small-signal stability margin of droop-based islanded microgrids," *IEEE Trans. Ind. Appl.*, vol. 54, no. 3, pp. 2821–2833, May/Jun. 2018.

[14] J. He, Y. W. Li, and F. Blaabjerg, "An enhanced islanding microgrid reactive power, imbalance power, and harmonic power sharing scheme," *IEEE Trans. Power Electron.*, vol. 30, no. 6, pp. 3389–3401, Jun. 2015.

[15] M. S. Golsorkhi and D. D.-C. Lu, "A decentralized control method for islanded microgrids under unbalanced conditions," *IEEE Trans. Power Del.*, vol. 31, no. 3, pp. 1112–1121, Jun. 2016.

[16] P. P. Vergara, J. C. López, M. J. Rider, and L. C. D. Silva, "Optimal operation of unbalanced three-phase islanded droop-based microgrids," *IEEE Trans. Smart Grid*, vol. 10, no. 1, pp. 928–940, Jan. 2019.

[17] A. Vijay, S. Doolla, and M. C. Chandorkar, "Varying negative sequence virtual impedance adaptively for enhanced unbalanced power sharing among dgs in islanded AC microgrids," *IEEE Trans. Energy Convers.*, vol. 36, no. 4, pp. 3271–3281, Dec. 2021.

[18] E. Alizadeh, A. M. Birjandi, and M. Hamzeh, "Triple-harmonic-droop control strategy for accurate harmonic power sharing in low-voltage islanded microgrids," *IET Gener., Transmiss. Distrib.*, vol. 15, no. 11, pp. 1740–1751, 2021.

[19] T. Caldognetto, H. Abedini, and P. Mattavelli, "A per-phase power controller for smooth transitions to islanded operation," *IEEE Open J. Power Electron.*, vol. 2, pp. 636–646, 2021.

[20] W. T. Elsayed, H. Farag, H. H. Zeineldin, and E. F. El-Saadany, "Dynamic transitional droops for seamless line-switching in islanded microgrids," *IEEE Trans. Power Syst.*, vol. 36, no. 6, pp. 5590–5601, Nov. 2021.

[21] D. G. Photovoltaics and E. Storage, IEEE Standard for Interconnection and Interoperability of Distributed Energy Resources with Associated Electric Power Systems Interfaces, IEEE Standard, pp. 1547–2018, Apr. 2018.

[22] R. Razi, H. Iman-Eini, and M. Hamzeh, "An impedance-power droop method for accurate power sharing in islanded resistive microgrids," *IEEE Trans. Emerg. Sel. Topics Power Electron.*, vol. 8, no. 4, pp. 3763–3771, Dec. 2020.

[23] W. Yao, M. Chen, J. Matas, J. M. Guerrero, and Z.-M. Qian, "Design and analysis of the droop control method for parallel inverters considering the impact of the complex impedance on the power sharing," *IEEE Trans. Ind. Electron.*, vol. 58, no. 2, pp. 576–588, Feb. 2011.

[24] M. Aquib, N. Parth, S. Doolla, and M. C. Chandorkar, "An adaptive droop scheme for improving transient and steady-state power sharing among distributed generators in islanded microgrids," *IEEE Trans. Ind. Appl.*, vol. 59, no. 4, pp. 5136–5148, Jul./Aug. 2023.

[25] J. Zhang, J. Shu, J. Ning, L. Huang, and H. Wang, "Enhanced proportional power sharing strategy based on adaptive virtual impedance in low-voltage networked microgrid," *IET Gener., Transmiss. Distrib.*, vol. 12, no. 11, pp. 2566–2576, 2018.

[26] J. M. Rey, C. X. Rosero, M. Velasco, P. Martí, J. Miret, and M. Castilla, "Local frequency restoration for droop-controlled parallel inverters in islanded microgrids," *IEEE Trans. Energy Convers.*, vol. 34, no. 3, pp. 1232–1241, Sep. 2019.

[27] M. M. A. Abdelaziz, H. E. Farag, E. F. El-Saadany, and Y. A.-R. I. Mohamed, "A novel and generalized three-phase power flow algorithm for islanded microgrids using a newton trust region method," *IEEE Trans. Power Syst.*, vol. 28, no. 1, pp. 190–201, Feb. 2013.

[28] C. Li, S. K. Chaudhary, M. Savaghebi, J. C. Vasquez, and J. M. Guerrero, "Power flow analysis for low-voltage AC and DC microgrids considering droop control and virtual impedance," *IEEE Trans. Smart Grid*, vol. 8, no. 6, pp. 2754–2764, Nov. 2017.

[29] G. Raman and J. C.-H. Peng, "Mitigating stability issues due to line dynamics in droop-controlled multi-inverter systems," *IEEE Trans. Power Syst.*, vol. 35, no. 3, pp. 2082–2092, May 2020.

[30] IEEE Standard for Interconnecting Distributed Resources with Electric Power Systems," IEEE Standard 1547-2003, 2003.

[31] Y. Song, S. Sahoo, Y. Yang, and F. Blaabjerg, "Stability constraints on reliability-oriented control of AC microgrids–theoretical margin and solutions," *IEEE Trans. Power Electron.*, vol. 38, no. 8, pp. 9459–9468, Aug. 2023.

[32] A. M. Pasha et al., "Enhanced transient response and seamless interconnection of multi-microgrids based on an adaptive control scheme," *IET Renewable Power Gener.*, vol. 15, no. 11, pp. 2452–2467, 2021.

[33] A. Lasheen, M. E. Ammar, H. H. Zeineldin, A. Al-Durra, M. F. Shaaban, and E. El-Saadany, "Assessing the impact of reactive power droop on inverter based microgrid stability," *IEEE Trans. Energy Convers.*, vol. 36, no. 3, pp. 2380–2392, Sep. 2021.

[34] R. Tanabe and A. S. Fukunaga, "Improving the search performance of shade using linear population size reduction," in *Proc. IEEE Congr. Evol. Comput.*, 2014, pp. 1658–1665.

[35] W.H. Kersting "Radial distribution test feeders," *IEEE Trans. Power Syst.*vol. 6, no. 3, pp. 975–985, 1991, doi: 10.1109/59.119237

[36] P. Gangwar, S. N. Singh, and S. Chakrabarti, "Network reconfiguration for the DG-integrated unbalanced distribution system," *IET Gener., Transmiss. Distrib.*, vol. 13, no. 17, pp. 3896–3909, 2019.

Dalia Yousri received the B.Sc. (Hons.), M.Sc. and the Ph.D. degrees in electrical engineering from Fayoum University, Fayoum, Egypt, in 2011, 2016 and 2020, respectively. She is currently an Assistant Professor with Electrical Engineering Department, Fayoum University, Fayoum, Egypt. Since 2022, she has been a Postdoctoral Fellow with the Advanced Power and Energy Research Center, Khalifa University, Abu Dhabi, UAE. Dr. Yousri was the recipient of the Award of Excellence in Scientific Research at Fayoum University for 2021. Additionally, being recognized in the world's top 2% scientists list by Stanford University. Her current research interests include integrated energy management systems, modeling, analysis, and control of microgrids, and applications of optimization techniques in renewable-energy-based systems. Acting as a reviewer for various reputed journals, such as the IEEE TRANSACTIONS ON SUSTAINABLE ENERGY, IEEE TRANSACTIONS ON ENERGY CONVERSION, IEEE ACCESS, *Elsevier Energy Conversion and Management*, *International Journal of Hydrogen Energy, and Applied Energy*.

Hany E. Z. Farag (Senior Member, IEEE) received the B.Sc. (Hons.) and M.Sc. degrees in electrical engineering from Assiut University, Assiut, Egypt, in 2004 and 2007, respectively, and the Ph.D. degree in electrical and computer engineering from the University of Waterloo, Waterloo, ON, Canada, in 2013. Since 2013, he has been with the Department of Electrical Engineering and Computer Science, Lassonde School of Engineering, York University, Toronto, ON, where he is currently an Associate Professor and York Research Chair in integrated smart energy grids. His current research interests include the integration of distributed and renewable energy resources, transportation electrification, green hydrogen generation and storage, modeling, analysis, and design of microgrids, and applications of multi-agent and blockchain technologies in smart grids. Dr. Farag is a Registered Professional Engineer in Ontario. He was the recipient of the Early Researcher Award (ERA) from the Government of Ontario.

Hatem H. Zeineldin (Senior Member, IEEE) received the B.Sc. and M.Sc. degrees in electrical engineering from Cairo University, Giza, Egypt, in 1999 and 2002, respectively, and the Ph.D. degree in electrical and computer engineering from the University of Waterloo, Waterloo, ON, Canada, in 2006. He was with Smith and Andersen Electrical Engineering Inc., North York, ON, Canada, where he was involved in projects involving distribution system designs, protection, and distributed generation. He was a Visiting Professor with the Massachusetts Institute of Technology, Cambridge, MA, USA. He is with Khalifa University of Science and Technology, Abu Dhabi, UAE, and on leave from the Faculty of Engineering, Cairo University, Giza, Egypt. His current research interests include distribution system protection, distributed generation, and microgrids. Dr. Zeineldin is currently the Editor of the IEEE TRANSACTIONS ON ENERGY CONVERSION.

Ehab El-Saadany (Fellow, IEEE) He was born in Cairo, Egypt, in 1964. He received the B.Sc. and M.Sc. degrees in electrical engineering from Ain Shams University, Cairo, Egypt, in 1986 and 1990, respectively, and the Ph.D. degree in electrical engineering from the University of Waterloo, Waterloo, ON, Canada, in 1998. He is currently an IEEE Fellow for his contributions in distributed generation planning, operation and control. He was a Professor with the ECE Department, University of Waterloo, till 2019, where he was the Director of the Power M.Eng. Program between 2010 and 2015. He is currently a Professor of the Department of Electrical Engineering and Computer Science and the Director of the Advanced Power and Energy Research Center (APEC), Khalifa University, Abu Dhabi, UAE. Dr. El-Saadany is an Internationally recognized expert in the area of sustainable energy integration and smart distribution systems. He is a Registered Professional Engineer in the Province of Ontario. He has graduated 33 Ph.D. and 22 M.Sc. students and authored or coauthored more than 450 international journal and conference papers in addition to three U.S. patents. His research interests include smart grid operation and control, microgrids, self-healing, cyber-physical security of smart grids, protection, power quality, embedded generation and transportation electrification. Dr. El-Saadany was the two-time recipient of Canada Research Chair Award in Energy Systems during 2009–2014, and Smart Distribution Systems during 2014–2018, Mission Innovation Champion Award in 2020, prestigious Khalifa Award in 2021, and the 2023 Mohamed Bin Rashid Medal for Scientific Excellence.